JOURNAL OF MATERIALS SCIENCE 27 (1992) 1240–1244

Residual stresses induced by laser coatings: phenomenological analysis and predictions

M. PILLOZ, J. M. PELLETIER
GEMPPM-CALFETMAT, UA 341, Bât. 403, INSA, 69 621 Villeurbanne Cedex, France
A. B. VANNES
MMP-CALFETMAT, UA 447, ECL, BP 163, 69 131 Ecully Cedex, France

Laser surface treatments induce, like any other surface treatment, thermal gradients and hence residual stresses. In the present work, these stresses are determined in the case of coatings of various metallic materials on two different substrates: a low carbon steel and an austenitic stainless steel. Qualitative analysis of experimental results is performed by using a phenomenological modelling based on a decomposition of the specimen into three different parts. A generalization is proposed, which allows simple predictions of the behaviour.

1. Introduction

Residual stresses have a critical influence on behaviour and lifetime of a machine part or a structural component, because they are superimposed upon external applied stresses, and hence they modify the real value of load in the part considered [1–3]. Coatings or surface alloying, performed by conventional processing or by high-energy beams, induce, like any other surface treatment, thermal, structural or chemical heterogeneities. Consequently residual stresses are observed after such treatments. A complete understanding of these laws is a prerequisite to the development of these technologies. This control could be achieved by modelling, for any given coating–substrate system and for any processing conditions, the obtained residual stress field. Predictions require knowledge of the thermophysical properties of the materials and their evolution as a function of temperature. Currently, there is a lack of experimental data, especially concerning alloys used for technical applications. This paper describes a phenomenological analysis, based on an experimental approach. Results concern cobalt-, nickel- and iron-based alloys, deposited on either an austenitic stainless steel or low-carbon steel. A generalization is proposed.

2. Experimental procedure

The coatings and the substrates had the composition listed in Table I.

Powder was injected into the laser beam and the following processing conditions were used: 4 kW CO_2 laser, supplied by CILAS, operating with a TEM 01 mode; output power between 2300 and 2600 W; ZnSe lens, focusing distance 127 mm, defocusing distance 40 mm; lateral powder projection nozzle; protecting gas nitrogen; sample scanning speed in the range 4–6.6 mm s^{-1}.

3. Results

Laser-sprayed coatings were about 2 mm wide. By performing parallel successive tracks, with a partial overlapping, large surfaces may be achieved, as illustrated in Fig. 1. A typical micrographic observation on a transverse cross-section is shown in Fig. 2: both coating and substrate are clearly observed. These coatings have been studied in detail elsewhere [4, 5]. A fine microstructure is observed and only equilibrium phases are obtained after solidification. Furthermore, the determination of the residual stress field was performed using a destructive testing method [6–8], in a large variety of metals and alloys [5, 6, 9, 10]. Indeed about 50 systems were analysed. Figs 3–5 show some representative examples. σ_L and σ_T are the average values of longitudinal and transverse stresses, respectively, in the (L, T) plane.

The main results may be summarized as follows:

(i) σ_L and σ_T are nearly equal. We will assume, in agreement with the beam theory, that the stress σ_3 in a direction perpendicular to the specimen surface is

TABLE I Composition (in wt %) of materials used for coatings and substrates

		Fe	C	Co	Cr	Ni	W	Si	Mn	S	Mo	B
Co	base	0.42	1.25	63	28.5	1.1	4.5	1.1	0.02	0.01	0.01	–
Ni	base			–	30	36	5	–	–	–	9	3
Steel	1010	bal.	0.1	–	–	0.1	–	0.3	0.5	0.02	–	–
Steel	304L	bal.	0.03	–	18	10	–	0.07	1.5	–	–	–

0022–2461

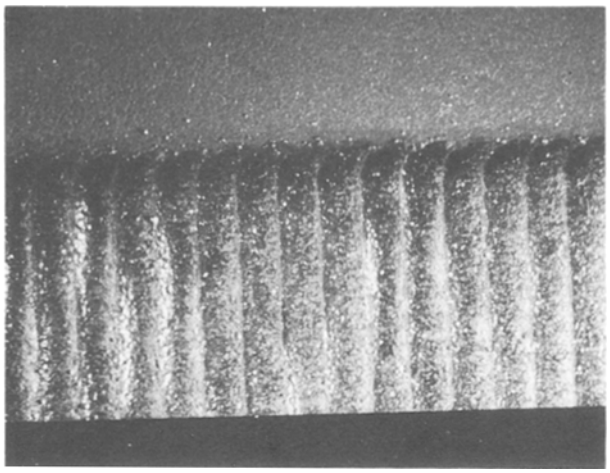

Figure 1 Example of coating obtained by laser treatment.

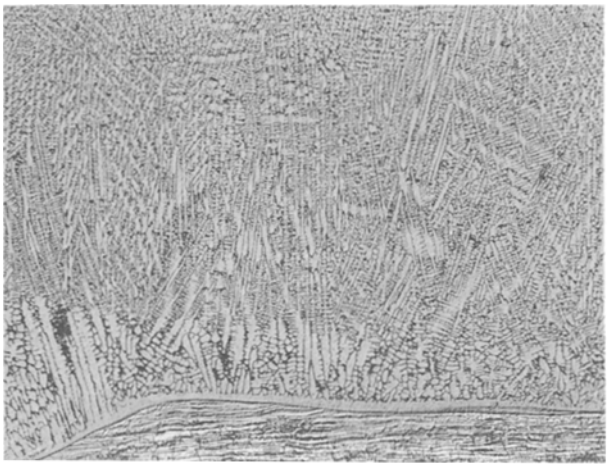

Figure 2 Example of micrography of a transverse cross-section; cobalt-based alloy coating on an austenitic stainless steel.

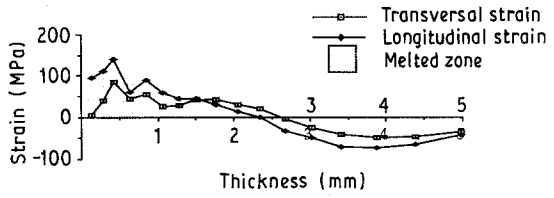

Figure 3 Residual stress field produced by a cobalt-based alloy coating (63Co–28Cr–W–(1.2C)) on an austenitic stainless steel 304L. $P = 2600$ W, $V = 6.6\ \text{mm s}^{-1}$.

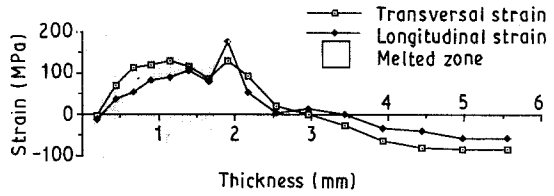

Figure 4 Residual stress field produced by a nickel-based alloy coating (36Ni–30Cr–20Fe–Mo–W–B–(1.00C)) on an austenitic stainless steel 304L. $P = 2300$ W, $V = 6.6\ \text{mm s}^{-1}$.

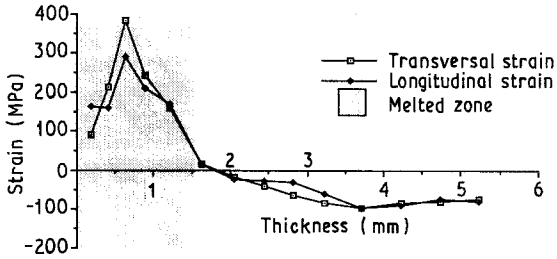

Figure 5 Residual stress field produced by a nickel-based alloy coating (36Ni–30Cr–20Fe–Mo–W–B–(1.00C)) on a low-carbon steel XC10. $P = 2300$ W, $V = 6.6\ \text{mm s}^{-1}$.

negligible, due to the symmetry of both sample shape and treatment processing.

(ii) For a given metallurgical state, the residual stress variations are small. Therefore the average value is significant.

(iii) Sharp transitions are observed between the different zones.

(iv) Coatings obtained with materials used for technological applications are almost always in tension. So the real value of load in these parts will be enhanced by these internal stresses.

4. Phenomenological modelling

4.1. Equivalent stresses; block scheme

Referring to Von Mises's criterion [3, 11–13] and taking into account the previous observations, the equivalent stress, σ_E is given by

$$2\sigma_E^2 = (\sigma_L - \sigma_T)^2 + (\sigma_T - \sigma_3)^2 + (\sigma_3 - \sigma_L)^2 \quad (1)$$

hence $\sigma_E = \sigma_L = \sigma_T$ because $\sigma_3 = 0$.

Experimental residual stress fields are then schematized as shown in Figs 6 and 7, corresponding to

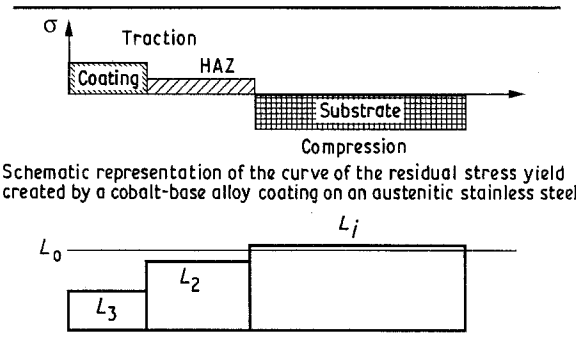

Figure 6 Block scheme associated with residual stress fields (cf. Fig. 3).

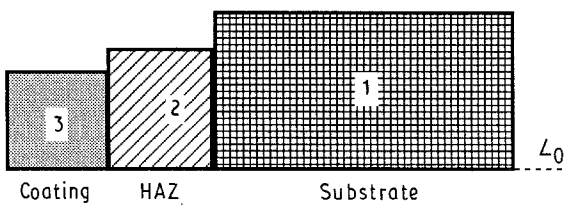

Figure 7 Block scheme associated with residual stress fields (cf. Fig. 5).

Figs 3 and 5, respectively. Assuming a continuity between the different parts, the equivalent length, L_e, corresponding to the whole sample, is obtained, for each block, by developing an elastic deformation, ε_i. The final length of a block, L_i, is then given by the summation of this deformation with the length obtained without any load. Hooke's law can be written

$$\sigma_i = E_i \varepsilon_i \quad (2)$$

where E_i is the longitudinal elastic modulus of part i.

4.2. Analysis of the residual stress development

4.2.1. Stainless steel substrate

To understand the stress origin requires an analysis of the complete heat-treatment cycle. Let us, for example, consider the configuration shown in Fig. 7: three blocks may be considered.

Block 1, which corresponds to the substrate. There was no irreversible effect during the heat cycle.

Block 2, which refers to the heat-affected zone of the substrate, in which metallurgical transformations and/or thermo-mechanical deformations occurred. In this austenitic stainless steel, only a creep phenomenon may be induced by thermal gradients during either heating or cooling. These gradients may be estimated from computing programs [14, 15]. Owing to the short duration of this cycle (about 1 s), we assume that creep occurs only in the temperature range (700 °C–T_M), where T_M is the melting temperature, and the average temperature is then about 1075 °C. Therefore, due to the thermal expansion of Block 2, the length of part 2 should be given, at the beginning of the coating processing, by $(L_0 + a_2 \times 1075)$, where a_2 is the thermal expansion coefficient of Block 2. However, in this temperature range, the flow stress of the austenitic stainless steel is very small and therefore continuity with the unheated substrate will induce a pronounced creep and the length of L_2 will remain nearly constant, to L_0.

Block 3, associated with the coating, does not exist during heating. In the liquid state, its length corresponds to the underlying block, i.e. Block 2 (length L_0), but with a temperature nearly equal to its melting point (1400–1500 °C).

Therefore residual stresses will be mainly created during cooling after the coating process. Let us analyse the behaviour of the different parts during this stage.

Block 1 remains unchanged, at L_0. Owing to the absence of any plastic deformation, the initial value is again obtained after the thermal cycle.

Block 2: no metallurgical transformation occurs during cooling, and therefore its final length is simply given by

$$L_2 = L_0(1 - a_2 \times 1075) \quad (3)$$

The value of a_2 was determined experimentally, as shown in Fig. 8; a is the integral coefficient defined by

$$a = \frac{L(T) - L_0}{L_0(T - T_0)} \quad (4)$$

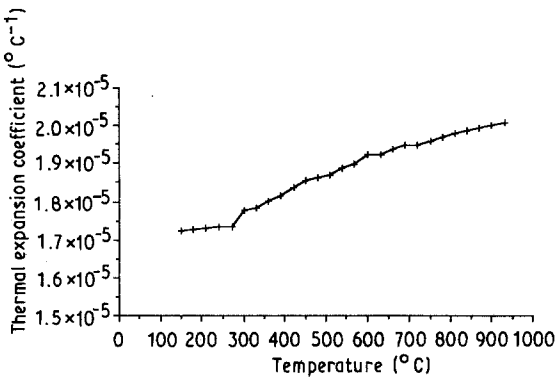

Figure 8 Integral linear thermal expansion coefficient versus temperature for the austenitic stainless steel.

where L_0 is the initial length at T_0 and $L(T)$ the value at temperature T. For $\Delta T = 1075$ °C, we obtained $a_2 = 20 \times 10^{-6}$ K^{-1}.

Finally, the length L_e, of the sample is given by the relation

$$L_e = L_3 + \varepsilon_3 = L_2 + \varepsilon_2 = L_0 + \varepsilon_1 \quad (5)$$

which takes into account both elastic accommodation and continuity conditions. Young's modulus values were determined, at room temperature, by a vibration testing method [5]: $E_1 = E_2 = 190\,000$ MPa; $E_3 = 220\,000$ MPa. Then the equilibrium equation becomes

$$\begin{aligned} L_e &= L_0(1 - a_3 \times 1450) + \frac{\sigma_3}{E_3} \\ &= L_0(1 - a_2 \times 1075) + \frac{\sigma_2}{E_2} \\ &= L_0 + \frac{\sigma_1}{E_1} \end{aligned} \quad (6)$$

and the different values are $L_3 < L_2 < L_0$. This result is in agreement with the experimental determination. It is obvious that this approach is only a rough approximation, because plastification effects induced during cooling may induce modulus changes and only elastic phenomena are considered. However, a qualitative agreement is observed.

4.2.2. Low-carbon steel

Phenomena occurring during heating are nearly the same as those obtained previously: the only transformation observed is the allotropic transformation in Block 2, with the formation of austenite [15–17]. Location of the boundary between the substrate and the heat-affected zone depends on the considered critical temperature: values between A_{c3} and A_{c1} (about 700 and 1000 °C, respectively) may be taken, due to the shift which could be induced by the rapid heating [18]. However in any case, creep will occur during this stage.

During cooling, behaviour of Blocks 1 and 3 is identical to the previous case. On the other hand, a new phenomenon arises in Block 2: the transformation of austenite into a mixture of ferrite and

pearlite (or bainite) in the temperature range 500–700 °C, or into an acicular ferrite by a displacive transformation in the temperature range 400–300 °C. Owing to the high quenching rate and to the observed residual stress field, this second hypothesis appears to be the more realistic. Therefore, three different steps have to be distinguished during the cooling of Block 2.

(a) First stage: from the end of the heating (average temperature estimated to about 1200 °C) [5] down to about 300 °C. Then the length, L', is given by

$$L' = L_0[1 - a' \times (1200 - 300)] = 0.9865\, L_0 \quad (7)$$

with $a' = 15 \times 10^{-6}\ K^{-1}$ [5].

(b) Second stage: a martensitic transformation occurs, with a progressive volume increase. For the given carbon concentration, this volume increase may be taken equal to about 1.5% and consequently the obtained length value, L'', at end of this step may be written

$$L'' = 1.015 \times L' = 1.001 \times L_0 \quad (8)$$

so the plastification phenomena will be negligible.

(c) Third step: from 300 °C down to room temperature. The final length, L_2, is then given by

$$L_2 = L'(1 - a_2 \times 300) = 0.9961\, L_0 \quad (9)$$

with $a = 13 \times 10^{-6}\ K^{-1}$. To summarize, we have $L_3 (= 0.9728\, L_0) < L_2 (= 0.9961\, L_0) < L_1 \approx L_0$.

Analysis of these two typical examples reveals that this phenomenological approach describes fairly well the process which induces the residual stress field. Three main conclusions may be drawn.

1. Heating induces a creep phenomenon in the heat-affected zone. Therefore, to assume a constant length in this zone appears realistic. This hypothesis is also confirmed by other studies [19, 20].

2. The differences in thermal expansion coefficients are the main factors which create residual stresses. Plastification effects during cooling have only a secondary influence, probably on the magnitude of these stresses, but not on their sign.

3. The delimitation of the different blocks is based on the thermal gradients.

5. Generalization

Generally, the formation of a metallic coating on a substrate induces the creation of three different zones, which may be treated as three separate parts, as shown above.

Part 1: the substrate. Effects induced by the thermal cycle are negligible. It may be assumed that the temperature remains constant and equal to the initial value T_1. Modulus of elasticity is E_1.

Part 2: the heat-affected zone. The heat cycle, $T(t)$, at any point in this zone causes structural changes. This cycle is determined by laser heating or by any other energy source. A critical temperature, T_c, may be defined; above this temperature different kinds of phenomena may be achieved: microstructural modifications (allotropic transformations, solution or precipitation reactions, recovery, recrystallization and grain growth, structural relaxation or crystallization in amorphous materials); plastic deformations induced by thermo-mechanical effects, etc.

The average temperature in this part is T_2 and E_2 is the Young's modulus. We define $\Delta T_2 = T_2 - T_1$.

Part 3: the coating, or, more generally, the melted zone, characterized by the solidification temperature T_{M3} and by the modulus E_3. Let us define $\Delta T_3 = T_{M3} - T_1$. As shown above, due to continuity and equilibrium conditions, the equivalent equilibrium length L_e, is given by

$$L_e = L_3 + \frac{\sigma_3}{E_3} = L_2 + \frac{\sigma_2}{E_2} = L_1 + \frac{\sigma_1}{E_1} \quad (10)$$

It is well known that a possible method to improve mechanical behaviour and especially fatigue strength, is to add compressive residual stresses in the surface layer (Part 3) ($\sigma_3 < 0$). In these conditions the overall equilibrium of the specimen induces tensile stresses in the underlying zone (Part 2) ($\sigma_2 > 0$). These conditions can be written $(\sigma_3/E_3) < 0$, $(\sigma_2/E_2) > 0$. So it may be predicted that a fatigue strength improvement requires that $L_3 > L_2$, $L_2 < L_0$.

Different values of a (thermal linear expansion coefficient) and T_M (melting temperature) are listed in Table II, for classical materials. Some cases appear to be of interest.

(i) The formation of a coating with a low coefficient of thermal expansion (a_3) (chromium or manganese for example), and with a low melting point (T_M) (unfortunately this condition is not fulfilled for these two metals). So an alternative has to be found.

(ii) Utilization of a substrate with a high thermal expansion coefficient (aluminium or magnesium for example), combined with a high value of T_2 (not true for aluminium or magnesium). Hence a new problem occurs.

Let us, for example, consider the case of a pure iron, nickel or cobalt coating on an austenitic stainless steel. Values are as follows: $\Delta T_3 = 1500$ °C and $\Delta T_2 = 1100$ °C. Then the condition is given by $(a_3/a_2) < 0.83$; as $a_2 = 20 \times 10^{-6}\ K^{-1}$ we obtain

TABLE II Melting temperature and average linear thermal expansion coefficients of some metals

	Ag	Al	Au	Co	Cr	Cu	Fe	Mg	Mn	Mo	Ni
T_M(°C)	961	660	1063	1495	1875	1083	1536	650	1245	2610	1453
a($10^{-6}\ K^{-1}$)	19,7	22	14,2	12,5	6,2	16,4	12,6	26,1	22	5,1	13,3

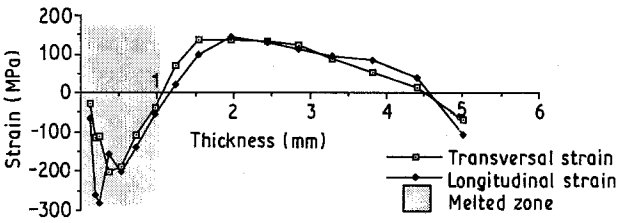

Figure 9 Residual stress field produced by a pure iron coating (99 Fe) on an austenitic steel 304L. $P = 2300$ W, $V = 6.6$ mm s^{-1}.

$a_3 < 14.6 \times 10^{-6}$ K^{-1}. Therefore a coating of pure iron, cobalt or nickel on this austenitic stainless steel should induce compressive residual stresses. Experimental results (Fig. 9) are in close agreement with this prediction. So this condition appears to be a good choice criterion. Other experiments should, however, be performed to confirm this conclusion.

In materials commonly used for technical applications, various phenomena must also be taken into account.

(a) In some alloys, phase transformations can occur during the heat cycle, during either heating or cooling. Owing to the short duration of this cycle, this phenomenon concerns mainly transformations without diffusion; indeed time allowed for diffusion is not long enough to enable significant changes, especially in substitutional alloys. The case of carbon atoms in solid solution (in interstitial position) in iron is, however, an important exception, as shown by Ashby and Easterling [15]. Some of the changes are diffusion controlled: the dissolution of cementite and the homogenization of austenite for example. For these, the extent of the change depends on the total number of diffusive jumps which take place during the cycle and hence on the diffusion distance λ, given by [15]

$$\lambda^2 = 2\int_0^{\infty} D\,dt \qquad (11)$$

where D is the diffusion coefficient, which is temperature dependent. This can be approximated for the laser heat cycle by [15]

$$\lambda^2 = 2D_0\alpha\tau\exp\left(\frac{Q}{RT_p}\right) \qquad (12)$$

where Q is the activation energy for the particular structural change, R is the gas constant, D_0, α, and τ are constants, and T_p is the peak temperature.

Calculations, as well as experimental results, indicate that the diffusion phenomenon of carbon in a low-carbon steel is significant and consequently a modification of parameters, especially of a, may be induced. However, in austenitic stainless steels, it may be assumed that the magnitude of this effect is negligible.

(b) Creep may occur during the heat cycle. Prediction of its magnitude is difficult to perform, because various parameters must be known: in addition to the complete heat cycle, the knowledge of the variation as a function of temperature of different properties, such as Young's modulus and elastic limit, are required. Precise values have not yet been reported in the literature and hence computation results are limited.

6. Conclusion

Reproducibility of residual stress fields obtained after laser coating make it possible to determine the pertinent parameters of the materials. By using a phenomenological approach based on a decomposition of the specimen into three parts, it is shown that three phenomena have to be taken into account.

1. Thermal contraction effects in the different blocks: they determine the sign of the residual stresses.
2. Creep in heat-affected zone: sign and level of stresses depend on its magnitude.
3. Thermal gradients induced by laser heating: they influence the dimension of each block.

From these parameters and with knowledge of thermophysical properties of the materials, a good qualitative prediction of residual stress fields produced by a given coating is then possible. This information is sufficient in a first approach, to choose appropriate materials. To improve the precision of the results, more precise computation codes have to be developed. Here the difficulty orginates from a lack of precise data concerning physical and mechanical properties of materials and especially concerning their temperature evolution.

References

1. W. CHENG and I. FINNIE, *Exp. Mech.* **6** (1986) 150.
2. A. B. VANNES, R. FOUGERES and M. THEOLIER, *Trait. Therm.* **87** (1974) 67.
3. A. B. VANNES, *Ann. Chim Fr.* **13** (1988) 211.
4. M. PILLOZ, C. SAHOUR, S. BONNET-JOBEZ, J. M. PELLETIER and A. B. VANNES, in "Proceedings of the 28th Special Steels Conference, 24–25 May 1989, Liège, Belgium (Cercle d'Etude des Metaux, Saint-Etienne, France).
5. M. PILLOZ, Thesis, INSA, Lyon, France (1990).
6. J. HERNANDEZ, Thesis, INSA, Lyon, France (1986).
7. J. HERNANDEZ, T. LATCHI, M. P. GENCE, C. BIGNON, M. BOIVIN, M. LARACINE, M. LORMAND and A. B. VANNES, *Mécan. Matér. Electr.* **415** (1986) 58.
8. M. LARACINE, C. BIGNON, M. LORMAND, J. HERNANDEZ and A. B. VANNES, *J. de Phys* **C7** (1988) 147.
9. C. CHABROL and A. B. VANNES, in "NATO ASI Series E: Applied Sciences", edited by C. W. Draper and R. Mazzoldi (Mathaus Nishoff, Dordrecht, NL, 1986) p. 435.
10. J. M. PELLETIER, S. JOBEZ, Q. SAIF, P. KIRAT and A. B. VANNES, *J. Mater. Engng*, in press.
11. A. B. VANNES, Thesis, INSA, Lyon, France (1978).
12. A. B. VANNES, in "Procédés électriques dans les traitements et revêtements de surface", edited by M. Dopee (EDF, Avon, 1989) p. 603.
13. A. J. FLETCHER, in "Thermal stresses ans strain generation in heat treatments" (Elsevier Applied Science, London, 1989) p. 11.
14. D. PERGUE, Thesis, INSA, Lyon, France (1987).
15. M. F. ASHBY and K. E. EASTERLING, *Acta Metall.* **32** (1984) 1935.
16. D. PERGUE, J. M. PELLETIER, F. FOUQUET and H. MAZILLE, *J. Mater. Sci.* **24** (1989) 4343.
17. C. CHABROL, Thesis, INSA, Lyon, France (1985).
18. D. FARIAS, S. DENIS and A. SIMON, in Proceedings of the 2nd International Seminar "Surface Engineering with High Energy Beams", Lisbon, Portugal, 25–27 September 1989 (CEMUL, Lisbon, Portugal, 1989) p. 139.
19. S. BONNET-JOBEZ, J. M. PELLETIER and A. B. VANNES, *Mécan. Matér. Electr.* **430** (1989) 39.
20. E. GAFFET, J. M. PELLETIER and S. BONNET-JOBEZ, *Acta Metall.* **37** (1989) 3205.

Received 23 November 1990
and accepted 10 April 1991